Rigorously conservative charge and current deposition in 3D cylindrical PIC

Yinjian Zhao[1] · Chen Cui[2] · Yuan Hu[3]

Abstract

A charge and current deposition method is presented for electromagnetic particle-in-cell simulations in 3D cylindrical coordinates using Yee's grid. The method is a direct extension of Villasenor and Buneman's current deposition method from Cartesian to 3D cylindrical coordinates, through computing the volumes swept by cylindrical sector charges over the current density surfaces. Along with Verboncoeur's correct volume terms for cylindrical coordinates, the method satisfies the continuity equation rigorously and eliminates edge errors.

Keywords Particle-in-cell (PIC) · Conservative deposition · 3D cylindrical coordinate · Yee's grid

1 Introduction

In 1992, Villasenor and Buneman proposed a current deposition scheme that satisfies the continuity equation rigorously in Cartesian coordinates for electromagnetic particle-in-cell (PIC) simulations [1] using finite-difference time-domain (FDTD) field solvers [2] on Yee's grid. Their algorithm has achieved a great success and has been widely applied in numerous works due to its simpleness and elegance. In 2001, Esirkepov proposed a new charge conserving scheme which generalizes Villasenor and Buneman's method to arbitrary particle form-factor in Cartesian coordinates [3].

Because substantial plasma facilities have a cylindrical shape, such as plasma sources [4,5], plasma torches [6,7], and plasma thrusters [8], it is naturally more convenient to carry out simulations in a cylindrical coordinate system for those applications. In cylindrical coordinates, however, both charge and current deposition schemes have some special difficulties. For charge deposition, Verboncoeur in 2001 proposed a symmetric spline weighting method, which eliminates the need for correction factors that are often applied in cylindrical coordinates to compensate for errors at the edge of the system [9]. For current deposition, extending Esirkepov's charge conserving current deposition method to 2D r–z is relatively straightforward, because the cells are still rectangular, as done by Davidson et al. [10].

2D r–z (axisymmetric) simulations are adequate in many situations, e.g. the plumes of plasma thrusters [11,12], where the plasma properties are uniform in the azimuthal direction. However, there are still considerable applications in which 3D effects cannot be ignored. For instance, the instability and turbulence enhanced anomalous plasma transport can significantly affect the performance of Hall thrusters [13,14]. Such anomalous transport is a 3D kinetic process, and a deep understanding of it requires high-fidelity full 3D kinetic simulations. Unfortunately, difficulties remain in the PIC scheme in the 3D cylindrical coordinate system, since the cells have cylindrical sector shapes. Greenwood et al. [15] developed charge conserving current weights for PIC in cylindrical coordinates. In their method, cells away from the cylindrical axis are mapped into cubes, and cells next to the cylindrical axis are mapped into triangular prisms.

In this paper, we present a method that extends Villasenor and Buneman's scheme [9] from Cartesian to 3D cylindri-

✉ Yuan Hu
  yhu@imech.ac.cn

  Yinjian Zhao
  yinjianzhao@lbl.gov

  Chen Cui
  cuichen@usc.edu

[1] Lawrence Berkeley National Laboratory, Berkeley, CA 94702, USA

[2] University of Southern California, Los Angeles, CA 90089, USA

[3] State Key Laboratory of High Temperature Gas Dynamics, Institute of Mechanics, Chinese Academy of Sciences, Beijing 100190, China

cal coordinates. The method computes the current density through the volumes swept by cylindrical sector charges over the current density surfaces. In the meantime, Verboncoeur's method [9] is applied to obtain the correct volumes for computing densities. Thus, the proposed method satisfies the continuity equation rigorously and eliminates the edge errors. To the best of our knowledge, there has been no work reported on a "direct" method that can compute the current deposition conservatively in 3D cylindrical PIC. The corresponding edge errors of the current deposition as well as the ways of eliminating them have not been studied yet.

It should be mentioned that a variety of body-fitted, curvilinear PIC schemes have been proposed to tackle problems with complex geometries, seeing [3,10,16–19] and references therein.

To guarantee the charge and current conservation, these curvilinear PIC schemes need a correction step for scattering typically in an ad hoc manner. Recently, Chacón and Chen [18] proposed a density-preserving algorithm which can rigorously scatters the charge and current densities to the grid in logical space, which is uniform and Cartesian. In contrast, the formulation presented in this work manipulates particles directly in physical space.

The rest of this paper is organized as follows: First, the charge deposition for 3D cylindrical PIC, applying the idea of Verboncoeur's method [9], is described and tested in Sect. 2. Then, the extended Villasenor and Buneman's current deposition method is derived and tested in Sect. 3. In Sect. 4, a full PIC simulation of an equilibrium pitch is chosen to further indicate the correctness of the current deposition method. At last, conclusion and possible future works are given in Sect. 5.

2 Charge deposition

In the 3D (r, ϕ, z) cylindrical coordinate system, we apply a mesh system with index i for r, j for ϕ, and k for z. Indices i, j, k range from 0 to N_r, N_ϕ, and N_z, respectively. We assume that cells are around by grid points, and the charge density values are defined on the grid points, as illustrated by Fig. 1. Thus, there are $N_r + 1$ grid points and N_r cells along r; $N_\phi + 1$ grid points and $N_\phi + 1$ cells along ϕ (the extra one cell is due to the periodic nature in ϕ); and $N_z + 1$ grid points and N_z cells along z. When $i = 0$, $r_0 \equiv 0$, which denotes the grid points on the $r = 0$ axis. If uniform cells are used, the cell sizes Δr, $\Delta \phi$, and Δz are all constants, thus $r_i = i\Delta r$, $\phi_j = j\Delta \phi$, $z_k = k\Delta z$, and $\Delta \phi = 2\pi/(N_\phi + 1)$. Note that all arrays defined on the grid points have a property: for any index k, when $i = 0$, all $j = 0, 1, 2, \ldots, N_\phi$ indices indicate the same grid point on the $r = 0$ axis, so these array values should be the same.
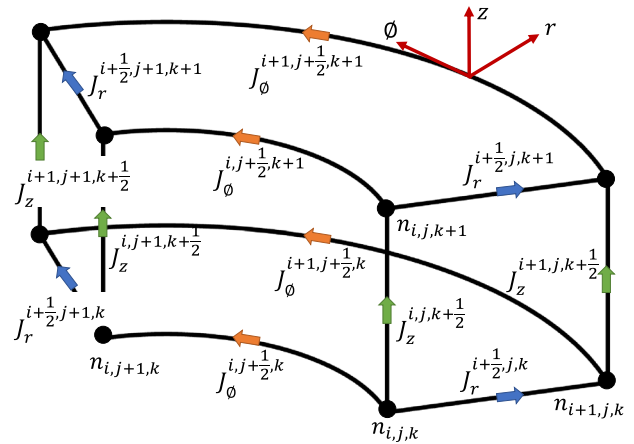

Fig. 1 Illustration of Yee's grid in 3D cylindrical coordinates

The deposition of the number density $n(i, j, k)$ is described as follows: For convenience, we first define the linear weighting "length" functions in r, ϕ, and z, according to [9],

$$L_r^-(i) = \int_{r_{i-1}}^{r_i} r \frac{r - r_{i-1}}{r_i - r_{i-1}} dr = \frac{(3i-1)\Delta r^2}{6}, \quad L_r^-(0) \equiv 0, \tag{1}$$

$$L_r^+(i) = \int_{r_i}^{r_{i+1}} r \frac{r_{i+1} - r}{r_{i+1} - r_i} dr = \frac{(3i+1)\Delta r^2}{6}, \quad L_r^+(N_r) \equiv 0, \tag{2}$$

$$L_\phi^-(j) = \int_{\phi_{j-1}}^{\phi_j} \frac{\phi - \phi_{j-1}}{\phi_j - \phi_{j-1}} d\phi = \frac{\Delta \phi}{2}, \tag{3}$$

$$L_\phi^+(j) = \int_{\phi_j}^{\phi_{j+1}} \frac{\phi_{j+1} - \phi}{\phi_{j+1} - \phi_i} d\phi = \frac{\Delta \phi}{2}, \tag{4}$$

$$L_z^-(k) = \int_{z_{k-1}}^{z_k} \frac{z - z_{k-1}}{z_k - z_{k-1}} dz = \frac{\Delta z}{2}, \quad L_z^-(0) \equiv 0, \tag{5}$$

$$L_z^+(k) = \int_{z_k}^{z_{k+1}} \frac{z_{k+1} - z}{z_{k+1} - z_k} dz = \frac{\Delta z}{2}, \quad L_z^-(N_z) \equiv 0, \tag{6}$$

where $\Delta r^2 \equiv (\Delta r)^2$. Then, taking indices i, j, and k as inputs for all L functions, we can obtain the cell volume term used for computing the density,

$$V_{i,j,k} = \sum_{-}^{+} L_r(i) L_\phi(j) L_z(k), \tag{7}$$

where the sum is over all combinations of the L functions with superscripts "−" and "+", i.e., eight terms in total. Similarly, one can obtain other volume terms, such as $V_{i+1,j,k}$, $V_{i,j+1,k+1}$, and so on.

From the perspective of the density deposition of one macroparticle in the loop over all macroparticles, denoting the position of the macroparticle p as (r_p, ϕ_p, z_p) and its weight as w_p, we first compute its linear weightings to r, ϕ, and z directions. Assume $r_p \in [r_i, r_{i+1})$, $\phi_p \in [\phi_j, \phi_{j+1})$,

and $z_p \in [z_k, z_{k+1})$, then denote the six fractions,

$$f_r^i = \frac{r_{i+1} - r_p}{r_{i+1} - r_i}, \quad f_r^{i+1} = \frac{r_p - r_i}{r_{i+1} - r_i}, \tag{8}$$

$$f_\phi^j = \frac{\phi_{j+1} - \phi_p}{\phi_{j+1} - \phi_j}, \quad f_\phi^{j+1} = \frac{\phi_p - \phi_j}{\phi_{j+1} - \phi_j}, \tag{9}$$

$$f_z^k = \frac{z_{k+1} - z_p}{z_{k+1} - z_k}, \quad f_z^{k+1} = \frac{z_p - z_k}{z_{k+1} - z_k}. \tag{10}$$

Therefore, the density deposition of the macroparticle p on the eight grid points around it can be expressed as

$$n_p^{i,j,k} = w_p \frac{f_r^i f_\phi^j f_z^k}{V_{i,j,k}},$$

$$n_p^{i,j+1,k+1} = w_p \frac{f_r^i f_\phi^{j+1} f_z^{k+1}}{V_{i,j+1,k+1}},$$

$$n_p^{i+1,j,k+1} = w_p \frac{f_r^{i+1} f_\phi^j f_z^{k+1}}{V_{i+1,j,k+1}},$$

$$n_p^{i+1,j+1,k} = w_p \frac{f_r^{i+1} f_\phi^{j+1} f_z^k}{V_{i+1,j+1,k}},$$

$$n_p^{i+1,j+1,k+1} = w_p \frac{f_r^{i+1} f_\phi^{j+1} f_z^{k+1}}{V_{i+1,j+1,k+1}},$$

$$n_p^{i+1,j,k} = w_p \frac{f_r^{i+1} f_\phi^j f_z^k}{V_{i+1,j,k}},$$

$$n_p^{i,j+1,k} = w_p \frac{f_r^i f_\phi^{j+1} f_z^k}{V_{i,j+1,k}},$$

$$n_p^{i,j,k+1} = w_p \frac{f_r^i f_\phi^j f_z^{k+1}}{V_{i,j,k+1}}. \tag{11}$$

Then, these n_p values should be accumulated to the density array n with the corresponding indices. Also note that if $j = N_r$, the index $j + 1$ should be replaced by 0 due to the periodic nature of the ϕ direction.

If uniform cells are used, the computation can be simplified. It is convenient to split V into V_r, V_ϕ, and V_z three components, e.g., $V_{i+1,j,k} = V_r^{i+1} V_\phi^j V_z^k$. Under these notations, we can obtain

$$V_r^i(i) = i\Delta r^2, \quad V_r^i(i = 0) \equiv \Delta r^2/6, \tag{12}$$

$$V_r^{i+1}(i) = (i+1)\Delta r^2, \quad V_r^{i+1}(i = N_r - 1) \equiv (3N_r - 1)\Delta r^2/6, \tag{13}$$

$$V_\phi^j(j) = V_\phi^{j+1}(j) = \Delta\phi, \tag{14}$$

$$V_z^k(k) = \Delta z, \quad V_z^k(k = 0) \equiv \Delta z/2, \tag{15}$$

$$V_z^{k+1}(k) = \Delta z, \quad V_z^{k+1}(k = N_z - 1) = \Delta z/2. \tag{16}$$

After computing the density array n and exiting the particle loop, for each k, one may want to update those j values
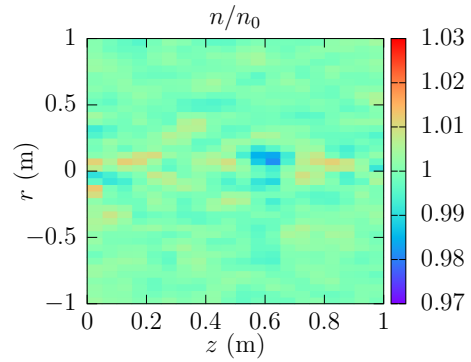

Fig. 2 Normalized number density n/n_0 on the r–z plane of $\phi = 0$ (labeled as $r > 0$) and $\phi = \pi$ (labeled as $r < 0$). $n_0 = N_p/\pi$ denotes the expected density value

when $i = 0$ to be their average, since they all denote the same physical grid point. At last, one can simply multiply n by the particle species charge q to obtain the charge density $\rho = qn$. Of course, if there are more than one species of particles, a superposition is needed, i.e., $\rho = \sum q_\alpha n_\alpha$, where α denotes the αth species.

2.1 Test

A test is done using $N_r = 20$, $N_\phi = 19$, $N_z = 20$, and the number of macroparticles $N_p = 2 \times 10^8$ with weight $w_p = 1$. These particles are randomly and uniformly distributed in the cylindrical domain, which ranges from $r = 0$ to $r = 1$ m and from $z = 0$ to $z = 1$ m. Uniform cell sizes are used, thus $\Delta r = 1/N_r = 0.05$ m, $\Delta\phi = 2\pi/(N_\phi + 1) = \pi/10$ rad, $\Delta z = 1/N_z = 0.05$ m.

As shown in Fig. 2, we can obtain a good uniform distribution of particles over the domain without systematic edge errors. The nonsystematic errors are relatively bigger near the axis, because there are less number of macroparticles per cell, due to smaller cell volumes, which is the nature of uniform cylindrical cells. If nonuniform radial cells are utilized, for example relatively longer cells in r near the axis, the errors near the axis would be reduced.

3 Current deposition

Assume a macroparticle p is located at (r_p, ϕ_p, z_p) at time t_n, and moves to (r'_p, ϕ'_p, z'_p) at time t_{n+1}. First, we only consider the situation in which $r_p, r'_p \in [r_i, r_{i+1})$, $\phi_p, \phi'_p \in [\phi_j, \phi_{j+1})$, and $z_p, z'_p \in [z_k, z_{k+1})$, i.e., p does not move out of a cell during timestep $\Delta t = t_{n+1} - t_n$. While the charge density ρ is defined on grid points, the current density components are defined on the edges of cells. J_r is defined at $(i + 1/2, j, k)$, J_ϕ is defined at $(i, j + 1/2, k)$, and J_z is defined at $(i, j, k + 1/2)$, as illustrated in Fig. 1. During
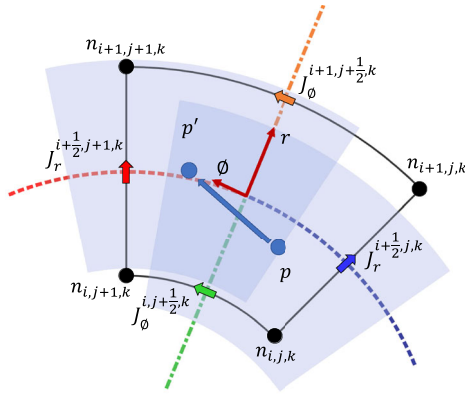
Fig. 3 Illustration of macroparticle motion on r–ϕ plane

the macroparticle motion from time t_n to t_{n+1}, the volumes swept by the cylindrical sector charge p over the current density surfaces can be expressed as follows.

First, take J_r as an example, as shown in Fig. 3, the portion of $J_r^{i+1/2,j+1,k}$ overlapped by p along ϕ direction is $\phi_p(t) + \Delta\phi/2 - \phi_{j+1/2}$, and that of $J_r^{i+1/2,j,k}$ is $\Delta\phi - (\phi_p(t) + \Delta\phi/2 - \phi_{j+1/2})$, and the corresponding arc lengths along ϕ can be obtained by multiplying the radius $r_{i+1/2}$, where the surfaces of $J_r^{i+1/2,j,k}$ and $J_r^{i+1/2,j+1,k}$ are located. Similarly, along z direction, the portion of $J_r^{i+1/2,j,k+1}$ is $z_p(t) + \Delta z/2 - z_{k+1/2}$ and that of $J_r^{i+1/2,j,k}$ is $\Delta z - (z_p(t) + \Delta z/2 - z_{k+1/2})$. Considering motion with constant velocity during the process, $r_p(t) = r_p + v_r t$, $\phi_p(t) = \phi_p + v_\phi t$, and $z_p(t) = z_p + v_z t$, where $v_r = (r_p' - r_p)/\Delta t$, $v_\phi = (\phi_p' - \phi_p)/\Delta t$ (note that the defined v_ϕ here has dimensions rad/s), and $v_z = (z_p' - z_p)/\Delta t$, we can obtain the volumes swept by the cylindrical sector charge over the surfaces of J_r,

$$
\mathcal{V}_{Jr}^{i+1/2,j,k}
= \int_0^{\Delta t} (\phi_{j+1} - \phi_p - v_\phi t) r_{i+1/2} (z_{k+1} - z_p - v_z t) v_r \, dt
$$

$$
\mathcal{V}_{Jr}^{i+1/2,j+1,k}
= \int_0^{\Delta t} (\phi_p - \phi_j + v_\phi t) r_{i+1/2} (z_{k+1} - z_p - v_z t) v_r \, dt.
$$

$$
\mathcal{V}_{Jr}^{i+1/2,j,k+1}
= \int_0^{\Delta t} (\phi_{j+1} - \phi_p - v_\phi t) r_{i+1/2} (z_p + z_k + v_z t) v_r \, dt,
$$

$$
\mathcal{V}_{Jr}^{i+1/2,j+1,k+1}
= \int_0^{\Delta t} (\phi_p - \phi_j + v_\phi t) r_{i+1/2} (z_p + z_k + v_z t) v_r \, dt. \quad (17)
$$

For J_ϕ, as illustrated by Fig. 3, the portion of $J_\phi^{i+1,j+1/2,k}$ overlapped by p along r direction is $r_p(t) + \Delta r/2 - r_{i+1/2}$, and that of $J_\phi^{i,j+1/2,k}$ is $\Delta r - (r_p(t) + \Delta r/2 - r_{i+1/2})$. The

portions along z are the same as those for J_r. Thus, the volumes swept by p over the surfaces of J_ϕ read

$$
\mathcal{V}_{J\phi}^{i,j+1/2,k} = \int_0^{\Delta t} (r_{i+1} - r_p - v_r t)(z_{k+1} - z_p - v_z t) v_\phi r_i \, dt,
$$

$$
\mathcal{V}_{J\phi}^{i+1,j+1/2,k} = \int_0^{\Delta t} (r_p - r_i + v_r t)(z_{k+1} - z_p - v_z t) v_\phi r_{i+1} \, dt,
$$

$$
\mathcal{V}_{J\phi}^{i,j+1/2,k+1} = \int_0^{\Delta t} (r_{i+1} - r_p - v_r t)(z_p - z_k + v_z t) v_\phi r_i \, dt,
$$

$$
\mathcal{V}_{J\phi}^{i+1,j+1/2,k+1} = \int_0^{\Delta t} (r_p - r_i + v_r t)(z_p - z_k + v_z t) v_\phi r_{i+1} \, dt.
$$

$$(18)$$

Note that v_ϕ should be multiplied by r_i for $V_{J\phi}^i$ terms and r_{i+1} for $V_{J\phi}^{i+1}$ terms accordingly in these integrals.

For J_z, special care should be taken for the radius used to multiply with the ϕ portions. Namely, for both portions, the dynamic radius $r_p(t)$, or equivalently the midpoint $(r_p + r_p')/2$, should be used in the integrals, as shown as follows:

$$
\mathcal{V}_{Jz}^{i,j,k+1/2} = \int_0^{\Delta t} (r_{i+1} - r_p - v_r t)(\phi_{j+1} - \phi_p - v_\phi t) r_p(t) v_z \, dt,
$$

$$
\mathcal{V}_{Jz}^{i+1,j,k+1/2} = \int_0^{\Delta t} (r_p - r_i + v_r t)(\phi_{j+1} - \phi_p - v_\phi t) r_p(t) v_z \, dt,
$$

$$
\mathcal{V}_{Jz}^{i,j+1,k+1/2} = \int_0^{\Delta t} (r_{i+1} - r_p - v_r t)(\phi_p - \phi_j + v_\phi t) r_p(t) v_z \, dt,
$$

$$
\mathcal{V}_{Jz}^{i+1,j+1,k+1/2} = \int_0^{\Delta t} (r_p - r_i + v_r t)(\phi_p - \phi_j + v_\phi t) r_p(t) v_z \, dt.
$$

$$(19)$$

After calculating the integrals, all the volumes are listed as follows:

$$
\mathcal{V}_{Jr}^{i+1/2,j,k} = (\phi^+ z^+ - \phi^+ \delta z/2 - z^+ \delta\phi/2 + \delta\phi\delta z/3)|\delta r|r_{i+1/2},
$$

$$
\mathcal{V}_{Jr}^{i+1/2,j+1,k} = (\phi^- z^+ - \phi^- \delta z/2 + z^+ \delta\phi/2 - \delta\phi\delta z/3)|\delta r|r_{i+1/2},
$$

$$
\mathcal{V}_{Jr}^{i+1/2,j,k+1} = (\phi^+ z^- + \phi^+ \delta z/2 - z^- \delta\phi/2 - \delta\phi\delta z/3)|\delta r|r_{i+1/2},
$$

$$
\mathcal{V}_{Jr}^{i+1/2,j+1,k+1} = (\phi^- z^- + \phi^- \delta z/2 + z^- \delta\phi/2 + \delta\phi\delta z/3)|\delta r|r_{i+1/2},
$$

$$(20)$$

$$
\mathcal{V}_{J\phi}^{i,j+1/2,k} = (r^+ z^+ - r^+ \delta z/2 - z^+ \delta r/2 + \delta r \delta z/3)|\delta\phi|r_i,
$$

$$
\mathcal{V}_{J\phi}^{i+1,j+1/2,k} = (r^- z^+ - r^- \delta z/2 + z^+ \delta r/2 - \delta r \delta z/3)|\delta\phi|r_{i+1},
$$

$$
\mathcal{V}_{J\phi}^{i,j+1/2,k+1} = (r^+ z^- + r^+ \delta z/2 - z^- \delta r/2 - \delta r \delta z/3)|\delta\phi|r_i,
$$

$$
\mathcal{V}_{J\phi}^{i+1,j+1/2,k+1} = (r^- z^- + r^- \delta z/2 + z^- \delta r/2 + \delta r \delta z/3)|\delta\phi|r_{i+1},
$$

$$(21)$$

$$
\mathcal{V}_{Jz}^{i,j,k+1/2} = (r^+ \phi^+ - r^+ \delta\phi/2 - \phi^+ \delta r/2 + \delta r \delta\phi/3)|\delta z|\tilde{r}_p,
$$

$$
\mathcal{V}_{Jz}^{i+1,j,k+1/2} = (r^- \phi^+ - r^- \delta\phi/2 + \phi^+ \delta r/2 - \delta r \delta\phi/3)|\delta z|\tilde{r}_p,
$$

$$
\mathcal{V}_{Jz}^{i,j+1,k+1/2} = (r^+ \phi^- + r^+ \delta\phi/2 - \phi^- \delta r/2 - \delta r \delta\phi/3)|\delta z|\tilde{r}_p,
$$

$$
\mathcal{V}_{Jz}^{i+1,j+1,k+1/2} = (r^- \phi^- + r^- \delta\phi/2 + \phi^- \delta r/2 + \delta r \delta\phi/3)|\delta z|\tilde{r}_p,
$$

$$(22)$$

where $r^+ \equiv r_{i+1} - r_p$, $r^- \equiv r_p - r_i$, $\phi^+ \equiv \phi_{j+1} - \phi_p$, $\phi^- \equiv \phi_p - \phi_j$, $z^+ \equiv z_{k+1} - z_p$, $z^- \equiv z_p - z_k$, $\delta r \equiv r'_p - r_p$, $\delta\phi \equiv \phi'_p - \phi_p$, $\delta z \equiv z'_p - z_p$, and $\widetilde{r}_p \equiv r_p + \delta r/2$.

After computing these volumes, their sums are needed to compute fractions,

$$\sum \mathcal{V}_{Jr} = r_{i+1/2}\Delta\phi\Delta z|\delta r|, \tag{23}$$

$$\sum \mathcal{V}_{J\phi} = \widetilde{r}_p\Delta r\Delta z|\delta\phi|, \tag{24}$$

$$\sum \mathcal{V}_{Jz} = \widetilde{r}_p\Delta r\Delta\phi|\delta z|. \tag{25}$$

Therefore, the current density due to p can be computed. For example,

$$J_{rp}^{i+1/2,j,k} = \frac{\mathcal{V}_{Jr}^{i+1/2,j,k}}{\sum \mathcal{V}_{Jr}}\frac{q_p w_p \delta r/\Delta t}{r_{i+1/2}\Delta r^2 \Delta\phi V_z^k}, \tag{26}$$

$$J_{\phi p}^{i,j+1/2,k} = \frac{\mathcal{V}_{J\phi}^{i,j+1/2,k}}{\sum \mathcal{V}_{J\phi}}\frac{q_p w_p \widetilde{r}_p\delta\phi/\Delta t}{\Delta\phi V_r^i V_z^k}, \tag{27}$$

$$J_{zp}^{i,j,k+1/2} = \frac{\mathcal{V}_{Jz}^{i,j,k+1/2}}{\sum \mathcal{V}_{Jz}}\frac{q_p w_p \delta z/\Delta t}{\Delta\phi \Delta z V_r^i}, \tag{28}$$

where V_r^i and V_z^k volume terms are computed according to Eqs. (12) and (15), respectively, and q_p denotes the particle species charge. Other current density terms can be obtained by changing the indices accordingly. Then, these J_p values can be accumulated to the current density array J with the corresponding indices.

At last, if the macroparticle moves out of a cell, a particle splitting procedure is needed as the one given in [1]. For example, for each macroparticle in the particle loop, we first call a subroutine in which we judge if the starting and ending positions of the macroparticle along r direction are within the same cell. If they are not, we can split the macroparticle into two, such that (r_p, ϕ_p, z_p) and (r''_p, ϕ''_p, z''_p) can be considered within one cell, (r''_p, ϕ''_p, z''_p) and (r'_p, ϕ'_p, z'_p) can be considered within the other cell, where r''_p equals the radius of the cell boundary that the macroparticle cross from r_p to r'_p, thus

$$\phi''_p = \phi_p + (\phi'_p - \phi_p)(r''_p - r_p)/(r'_p - r_p)$$
$$z''_p = z_p + (z'_p - z_p)(r''_p - r_p)/(r'_p - r_p). \tag{29}$$

Next, the one unsplitted or the two splitted macroparticles enter a similar subroutine for splitting in ϕ direction, and a similar subroutine for splitting in z direction.

3.1 Test

We apply the same setup and parameters used in Sect. 2.1. Additionally, we assign every macroparticle a constant velocity of $\boldsymbol{v} = (v_r, v_\phi, v_z)$, where $v_r = 0.001\Delta r/\Delta t$, $v_\phi =$

$0.001\Delta\phi/\Delta t$, and $v_z = 0.001\Delta z/\Delta t$. The timestep Δt is set to be 0.01 s. Unit particle charge and weight are used, i.e., $q_p = 1$, $w_p = 1$.

At time $t = 0$, the initial number density n_0 is computed, according to the method introduced in Sect. 2. Then, we move all macroparticles by $\boldsymbol{v}\Delta t$, where $\boldsymbol{v}$ is assumed at time $t = \Delta t/2$ according to the commonly used leap-frog scheme in PIC [20]. Next, the current density is computed using the old and new macroparticle positions. At time $t = \Delta t$, we compute the new number density n_1.

The results of J_r/J_{r0}, $J_\phi/J_{\phi 0}$, and J_z/J_{z0}, normalized by the expected constant values $J_{r0} = v_r N_p/\pi$, $J_{\phi 0} = r_i v_\phi N_p/\pi$, and $J_{r0} = v_z N_p/\pi$, respectively, are shown in Fig. 4. We can see that there is no systematic error and the nonsystematic errors are all limited within 4%. Note that in the code, the array of $J_r(i, j, k)$ corresponds to $J_r^{i+1/2,j,k}$ physically. Because $J_r^{N_r+1/2,j,k}$, i.e., $J_r(N_r, j, k)$, is defined outside of the domain, its values are zero; thus, $r = \pm 20$ is not shown in that plot. The same for the values of $J_z^{i,j,N_z+1/2}$, i.e., $J_z(i, j, N_z)$, $z = 20$ is not shown in that plot. Also note that $J_\phi^{0,j,k} = 0$ because the two volume terms $\mathcal{V}_{J\phi}^{i,j+1/2,k}$ and $\mathcal{V}_{J\phi}^{i,j+1/2,k+1}$ from Eq. (21) are zeros on axis ($i = 0$). Thus, these values are not shown in that plot as well.

More importantly, the conservation of the continuity equation is verified. We examine the following relative error,

$$\text{Error} = \left(\frac{n_1^{i,j,k} - n_0^{i,j,k}}{\Delta t} + \frac{r_{i+1/2}J_r^{i+1/2,j,k} - r_{i-1/2}J_r^{i-1/2,j,k}}{r_i\Delta r}\right.$$
$$\left. + \frac{J_\phi^{i,j+1/2,k} - J_\phi^{i,j-1/2,k}}{r_i\Delta\phi} + \frac{J_z^{i,j,k+1/2} - J_z^{i,j,k-1/2}}{\Delta z}\right)$$
$$\cdot\frac{\Delta t}{n_1^{i,j,k} - n_0^{i,j,k}}. \tag{30}$$

The result is plotted in Fig. 4 (lower right) for ranges i from 1 to $N_r - 1$, j from 0 to N_ϕ, and k from 1 to $N_z - 1$. As we can see, the relative error is very small, and for single particle tests, we only observe machine precision errors.

In addition, to indicate the importance of using those correct volume terms, such as V_r^i and V_z^k, as given in Eqs. (26), (27), and (28), we show the wrong current deposition result in Fig. 5. Taking J_ϕ as an example, we can see the edge errors can reach 30%, if the volume terms V_r^{i+1}, V_z^k, and V_z^{k+1} at the edges are not corrected as given in Eqs. (13), (15), and (16), respectively.

4 Full PIC test

To further test the correctness of the current deposition method in a full PIC simulation, the scenario of an equilibrium pitch is picked, in which an azimuthal magnetostatic field is excited by a cylinder of homogeneous plasma with

Fig. 4 Normalized current densities on the r–z plane of $\phi = 0$ (labeled as $r > 0$) and $\phi = \pi$ (labeled as $r < 0$), with a plot (lower right) of the error of the continuity equation
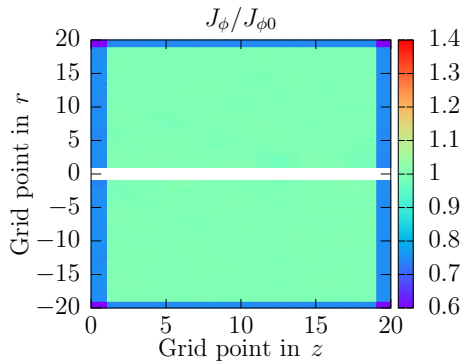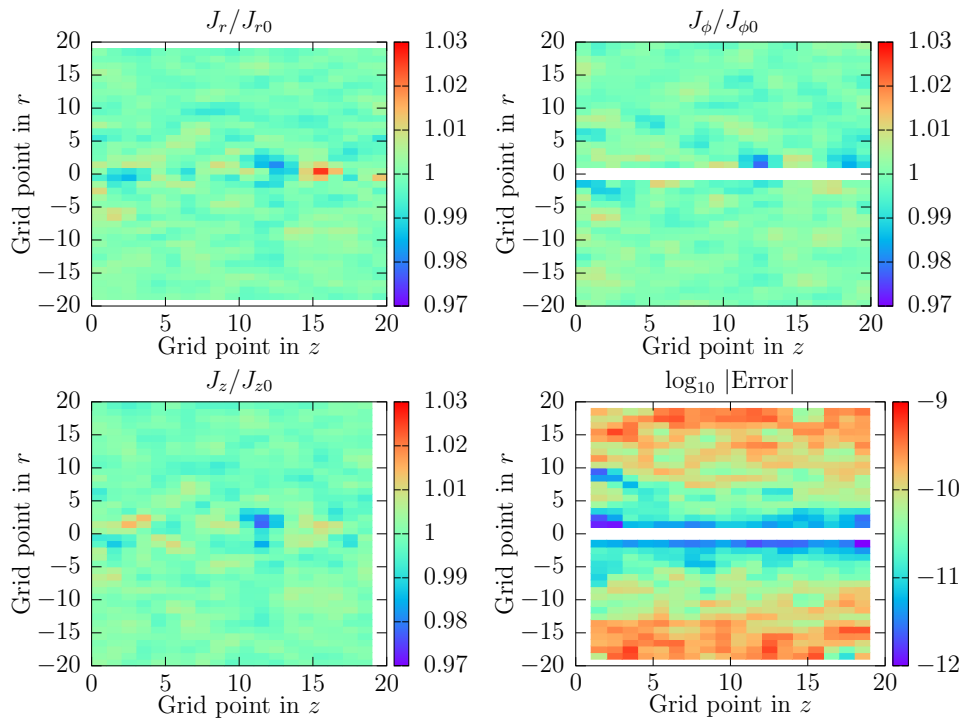

Fig. 5 Edge errors of J_ϕ when using the wrong volume terms

constant current density. The analytical solution of $B_\phi(r)$ is given by Bittencourt [21]

$$B_\phi(r) = \frac{\mu_0 I_0}{2\pi R^2} r \quad (r < R), \tag{31}$$

$$B_\phi(r) = \frac{\mu_0 I_0}{2\pi} \frac{1}{r} \quad (r \geq R), \tag{32}$$

where I_0 denotes the current, R denotes the cylinder radius, μ_0 is the vacuum permeability. Detailed parameters are chosen as follows.

A plasma of moving electrons and fixed ions are uniformly distributed spatially inside a cylinder with radius $R = 1$ m. We set the maximum azimuthal magnetic field $B_0 = 0.001$ T; thus, we can obtain the required plasma current, $I_0 = 2\pi R B_0 / \mu_0 \approx 5000$ A. Because ions are assumed

fixed, only electrons contribute to the current, if we let all electrons move with a constant velocity along the axis $v_0 = 10^4$ m/s, the electron (as well as ion) number density can be obtain from $n_e = n_i = I_0/(\pi R^2 e v_0) \approx 9.934 \times 10^{17}$ m^{-3}.

The number of electron and ion macroparticles is set to be 2×10^5, respectively. The axial velocity of all electrons is set to be $v_z = -v_0$. The other components of electron velocity are set to zero. In r, 1600 cells are used, i.e., $N_r = 1600$; In z and ϕ, 10 cells are used, respectively, i.e., $N_z = 10$ and $N_\phi = 9$, because B_ϕ is only a function of r, using less cells in z and ϕ can save computational time. The cell size are $\Delta r = 0.00625$ m and $\Delta z = 0.1$ m, which result in a domain size of 10 m in r and 1 m in z. We apply periodic boundary condition in z and reflective boundary condition in r. The simulation is stopped before the reflected wave reaches the range that we are interested in, i.e., $r \leq 2$ m. The timestep is chosen to be $\Delta t = 6.185 \times 10^{-12}$ s, and 7913 time steps are computed in total.

Initially, electrons and ions are set at exact positions such that there is zero net charge in the system, but because electrons have a constant axial velocity, the current is not zero. This initial current will excite electromagnetic waves, and the Maxwell equations are solved using the finite-difference time-domain (FDTD) method in 3D cylindrical coordinates [2], based on the current density obtained using the proposed method. Because we would like to keep the current density constant and avoid the disturbance on electrons due to the excited electromagnetic waves, the "field gather" process of a normal PIC is skipped, namely particles move with the
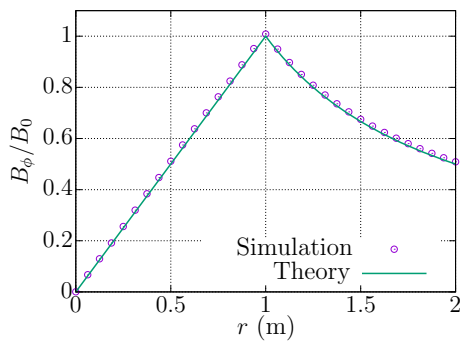
Fig. 6 Comparison of B_ϕ between simulation and theory

initial constant speed and are not affected by the fields. Electrons are pushed as normal at every time step using the Boris' cylindrical particle pusher [22].

Note that it is found in the PIC loop after calling the current deposition module, the J_z array may have different values at different j indices in ϕ at $i = 0$ (i.e., on the axis $r = 0$) for any k index in z. This difference would excite some nonphysical electromagnetic waves near the axis and thus makes the simulation unstable. Because when $i = 0$ all j grid points represent the same physical grid point, we set J_z to its mean value, i.e.,

$$J_z^{0,j,k+1/2} = \sum_{j=0}^{j=N_\phi} \frac{J_z^{0,j,k+1/2}}{N_\phi + 1}. \tag{33}$$

For those zero values of $J_\phi^{0,j+1/2,k}$, because they are not needed in the updating equations of the FDTD method, they can be kept as zeros.

The simulation result of $B_\phi(r)$ at the end of the simulation, i.e., at 7913 time step, is plotted in Fig. 6. The curve is obtained by averaging over all z and ϕ grid points, because B_ϕ remains uniform along z and ϕ with minor noise. From the figure, we can see that the simulation result matches well with the theory; thus, the correctness of the current deposition method in a full PIC is indicated.

5 Conclusion and future works

We present a method to compute the charge and current density deposition in 3D cylindrical PIC simulations on Yee's grid. It is motivated by the needs of high-fidelity PIC simulations for facilities with relatively simple cylindrical shapes where the 3D effects are important. The proposed algorithm satisfies the continuity equation rigorously and eliminates edge errors, by extending Villasenor and Buneman's method from Cartesian to cylindrical coordinates, and applying Verboncoeur's correct volume terms.

In this paper, only uniform cells and first-order particle form-factor are considered. One possible future work is to generalize the method by using nonuniform cells and higher-order particle form-factors. The other future work is to apply this method in a full 3D cylindrical PIC code and carry out more practical simulations. It will then be interesting to compare the accuracy and efficiency of our method with other relevant (perhaps more general) schemes like the curvilinear PIC [18] in some computationally demanding applications.

References

1. Villasenor J, Buneman O (1992) Rigorous charge conservation for local electromagnetic field solvers. Comput Phys Commun 69(2):306. https://doi.org/10.1016/0010-4655(92)90169-Y
2. Inan US, Marshall RA (2011) Numerical electromagnetics: the FDTD method, 1st edn. Cambridge University Press, Cambridge
3. Esirkepov T (2001) Exact charge conservation scheme for Particle-in-Cell simulation with an arbitrary form-factor. Comput Phys Commun 135(2):144. https://doi.org/10.1016/S0010-4655(00)00228-9
4. Chen FF, Boswell RW (1997) Helicons—the past decade. IEEE Trans Plasma Sci 25(6):1245
5. Shinohara S (2018) Helicon high-density plasma sources: physics and applications. Adv Phys X 3(1):1420424. https://doi.org/10.1080/23746149.2017.1420424
6. Trelles JP, Heberlein JVR, Pfender E (2007) Non-equilibrium modelling of arc plasma torches. J Phys D Appl Phys 40(19):5937. https://doi.org/10.1088/0022-3727/40/19/024
7. Bernardi D, Colombo V, Ghedini E, Mentrelli A (2005) Three-dimensional modeling of inductively coupled plasma torches. Pure Appl Chem 77(2):359. https://doi.org/10.1351/pac200577020359
8. Goebel DM, Katz I (2008) Fundamentals of electric propulsion: ion and hall thrusters. Wiley
9. Verboncoeur J (2001) Symmetric spline weighting for charge and current density in particle simulation. J Comput Phys 174(1):421. https://doi.org/10.1006/jcph.2001.6923
10. Davidson A, Tableman A, An W, Tsung F, Lu W, Vieira J, Fonseca R, Silva L, Mori W (2015) Implementation of a hybrid particle code with a PIC description in r–z and a gridless description in ϕ into OSIRIS. J Comput Phys 281:1063. https://doi.org/10.1016/j.jcp.2014.10.064
11. Hu Y, Wang J, Sun Q (2020) Geometrically self-similar ion acceleration in collisionless plasma beam expansion. Plasma Sources Sci Technol 29(12):125004
12. Hu Y, Huang Z, Cao Y, Sun Q (2021) Kinetic insights into thrust generation and electron transport in a magnetic nozzle. Plasma Sources Sci Technol 30(7):075006
13. Boeuf JP (2017) Tutorial: Physics and modeling of Hall thrusters. J Appl Phys 127(1):011101
14. Taccogna F, Minelli P (2018) Three-dimensional particle-in-cell model of Hall thruster: the discharge channel. Phys Plasmas 25(6):061208
15. Greenwood AD, Cartwright KL (2004) In: The 31st IEEE international conference on plasma science, 2004. ICOPS 2004. IEEE conference record—abstracts, p. 134. https://doi.org/10.1109/PLASMA.2004.1339653

16. Chacón L, Chen G, Barnes D (2013) A charge- and energy-conserving implicit, electrostatic particle-in-cell algorithm on mapped computational meshes. J Comput Phys 233:1. https://doi.org/10.1016/j.jcp.2012.07.042

17. Chen G, Chacón L (2015) A multi-dimensional, energy- and charge-conserving, nonlinearly implicit, electromagnetic Vlasov-Darwin particle-in-cell algorithm. Comput Phys Commun 197:73. https://doi.org/10.1016/j.cpc.2015.08.008

18. Chacón L, Chen G (2016) A curvilinear, fully implicit, conservative electromagnetic PIC algorithm in multiple dimensions. J Comput Phys 316:578. https://doi.org/10.1016/j.jcp.2016.03.070

19. Delzanno GL, Camporeale E, Moulton JD, Borovsky JE, MacDonald EA, Thomsen MF (2013) CPIC: A curvilinear particle-in-cell code for plasma-material interaction studies. IEEE Trans Plasma Sci 41(12):3577. https://doi.org/10.1109/TPS.2013.2290060

20. Birdsall CK, Langdon AB (1991) Plasma physics via computer simulation. Adam Hilger, Bristol

21. Bittencourt JA (2004) Fundamentals of plasma physics. Springer

22. Delzanno GL, Camporeale E (2013) On particle movers in cylindrical geometry for particle-in-cell simulations. J Comput Phys 253:259. https://doi.org/10.1016/j.jcp.2013.07.007

Publisher's Note Springer Nature remains neutral with regard to jurisdictional claims in published maps and institutional affiliations.